ELSEVIER

Journal of Magnetism and Magnetic Materials 166 (1997) 82–90

journal of magnetism and magnetic materials

Nanosize cobalt boride particles: control of the size and properties

C. Petit [a,b], M.P. Pileni [a,b,*]

[a] *Laboratoire SRSI, URA CNRS 1662, Université Pierre et Marie Curie, Bât. F, 4 Place Jussieu, F-75005 Paris, France*
[b] *CEA, DSM–DRECAM Service de Chimie Moléculaire, CE Saclay, F-91191 Gif sur Yvette Cedex, France*

Received 7 July 1995; revised 4 December 1995

Abstract

Cobalt boride is obtained by the reduction of cobalt (2-ethyl hexyl) sulfosuccinate, $Co(AOT)_2$, by sodium borohydride either in reverse micelles or in a diphasic system. In $Co(AOT)_2/Na(AOT)/H_2O$ reverse micellar solution, the size and polydispersity of the Co_2B particles is controlled by the size of the water droplets, which increases from 4 to 7.5 nm by increasing the water content. In a diphasic system of $Co(AOT)_2$/isooctane and sodium borohydride in aqueous solution, large and polydisperse particles of cobalt boride are formed ($\sim$ 10 nm), and their magnetization properties are presented. The smallest particles are in a superparamagnetic regime at room temperature, whereas the largest particles show ferromagnetic behavior.

Keywords: Nanoparticles; Cobalt; Superparamagnetism

1. Introduction

The synthesis of nanoparticles, characterized by a low size distribution, is a new challenge in solid state chemistry. Due to their small size, nanoparticles exhibit novel material properties that differ considerably from those of the bulk solid state [1]. Many reports on quantum size effects in the photochemistry of semiconductors [2,3] or the emergence of metallic properties with the size of the particles [4,5] have appeared in recent years. In this emerging field, finely divided magnetic nanoparticles are desirable due to their large domains of application, especially in high-density magnetic recording media or magnetically responsive fluids. The magnetic properties of these particles depend crucially on their shape or size [6].

In the last few years it has been well demonstrated that reverse micelles are good candidates for the production of nanoparticles [7]. Sodium bis(2-ethylhexyl) sulfosuccinate (AOT) is the surfactant most commonly used to form reverse micelles [8]. The ternary systems alkane/AOT/water present enormous advantages: they are spheroidal and monodisperse aggregates (size distribution around 20%) where water is readily solubilized in the polar core to form a 'water pool' characterized by the ratio of water to surfactant concentration ($w = [H_2O]/[AOT]$). In isooctane as the bulk solvent, the water pool radius, R_w, is found to be linearly dependent on the water content (R_w (Å) = 1.5 W) [9]. Another property of reverse micelles is their dynamic character; the water pools can exchange their contents by a

* Corresponding author. Fax: +33-1-4427-2515.

0304-8853/97/$17.00 Copyright © 1997 Elsevier Science B.V. All rights reserved.
PII S0304-8853(96)00621-X

collision process [8], which means that chemical reactions or coprecipitation between compounds solubilized in two different reverse micelles are possible. Hence, semiconductor [2,10] or metallic nanoparticles [4,11] can be synthesized in situ in AOT reverse micelles.

Recently Chen et al. [12,13] used reverse micelles (H_2O/AOT/isooctane and DDAB/toluene) to synthesize metallic cobalt fine particles. Cobalt particles are obtained from the reduction of cobalt salt by sodium borohydride. The metallic cobalt particles made in AOT reverse micelles were characterized by diameters of 3 and 4 nm, with superparamagnetic behavior. With DDAB reverse micellar solutions, the particles were larger (10 nm) and showed ferromagnetic behavior at room temperature [12,13]. In the latter system the size was controlled by changing the concentration of $CoCl_2$ in the microemulsion.

In this work, functionalized surfactant $Co(AOT)_2$ has been used to synthesize superparamagnetic nanoparticles of cobalt boride (Co_2B). In reverse micelles, the particle size is controlled by the size of the water droplet. The size of Co_2B varies from 4 to 7.5 nm. The absorption spectrum of Co_2B does not change with the size of the particles. Using a diphasic system made by mixing similar volumes of $Co(AOT)_2$ in isooctane to sodium borohydride aqueous solution, larger particles (10 nm) are obtained.

The magnetic properties have been determined at room temperature, and the magnetic size and susceptibility have been deduced from the magnetization curves.

2. Experimental

2.1. Products

All the materials were used without further purification. The $CoCl_2$ and AOT were purchased from Sigma, the isooctane from Fluka, and the sodium borohydride, $NaBH_4$, from Alpha Products. The synthesis of $Co(AOT)_2$ has been described elsewhere [14]. $Co(AOT)_2$ was used as a stock solution at 0.125 M in isooctane.

2.2. Apparatus

The reactions were carried out under an argon atmosphere. The organic solvents and Millipore deionized water were degassed with argon prior to use. The UV–vis absorption spectra were recorded on a conventional Varian Cary 1 spectrophotometer. Transmission electron microscopy (TEM) images and electron diffraction (SAD) patterns were obtained with a JEOL 100CX2 microscope. The solution was placed on a carbon-coated copper grid and evaporated under an argon atmosphere.

The magnetic studies were performed using a commercial alternating gradient magnetometer (Princeton Measurements Corporation, Micromag model 290) operating at room temperature in fields up to 2 T.

3. Treatments of the results

Histograms were obtained by measuring the diameters D_i of all the particles from different parts of the grid ($\times 160\,000$) for an average number of particles close to 500. The standard deviation, σ, is calculated from the following equation:

$$\sigma = \left\{ \sum \left[n_i (D_i - D)^2 \right] / [N-1] \right\}^{1/2},$$

where D is the average diameter and N is the number of particles. The first magnetization curve of each sample was simulated from the Langevin relationship [15]:

$$M(D) = M_s x\{\mathrm{ctnh}(\mu H/kT) - (kT/\mu H)\},$$

with $\mu = \mathscr{M}_s \pi D^3/6$. In a given field H, $M(D)$ is the magnetization of particles with diameter D. The total saturation magnetization of the overall particles, M_s, is related to the saturation magnetization of the bulk phase, $\mathscr{M}_s$, by the following relationship:

$$M_s = N \cdot \mathscr{M}_s,$$

where N is the number of particles. Assuming a log-normal size distribution, the magnetization of the particles at a given field, H, is [15]:

$$M = \int M(D)\, P(D)\, \mathrm{d}D,$$

where $P(D)$ is the number of particles of a given size, D.

4. Results and discussion

4.1. Synthesis and characterization of Co_2B particles in AOT reverse micelles

Mixed H_2O–$Co(AOT)_2$–Na(AOT)–isooctane reverse micelles are spherical water-in-oil droplets, whose size increases linearly with the water content, $w = [H_2O]/([Co(AOT)_2] + [Na(AOT)])$ [14].

The cobalt ions were reduced by mixing, volume to volume, two AOT reverse micellar solutions: one is made by 10^{-2} M $Co(AOT)_2$ and 0.23 M NaAOT in isooctane solution; and the other is 0.25 Na(AOT) in isooctane containing the desired amount of water and $NaBH_4$ as the reducing agent. The ratio $[BH_4^-]/[Co^{2+}]$ is kept equal to 4.

4.1.1. $5 \leq w \leq 10$

After mixing, the micellar solution remains optically clear and the color turns immediately from pink to black, indicating the formation of colloidal particles. Fig. 1 shows TEM images of the colloidal particles obtained in micelles at various water contents, w. An increase in the particle size from 4 to 7.5 nm is observed by increasing the water content from 5 to 10. The histograms show a size distribution of 25%. This polydispersity is of the same order of magnitude as that determined by X-ray scattering for AOT reverse micelles [16].

At water contents $w = 5$ and 7.5, the electron diffraction patterns reveal a crystalline order with spacings 2.5, 1.98 and 1.19 Å (Fig. 2A). These spacing values are similar to those given for Co_2B in Ref. [19]. Due to the small size of the nanoparticles, the diffraction lines of cobalt boride were always broad and diffuse.

At a water content $w = 10$, additional spacings to those corresponding to Co_2B are observed at 2.30 and 1.38 Å. Fig. 2B shows the spacings corresponding to Co_2O_3 and Co–O. From a comparison of these spacings it seems reasonable to conclude that Co_2O_3 is formed and not Co–O.

The formation of Co_2O_3 instead of Co–O is rather surprising, because the latter is usually more stable. This could be due to changes in the phase diagram when particles are made in reverse micelles. Similar behavior has been observed with other materials. It is well known that $Cd_yZn_{1-y}S$ and Fe–Cu alloys can not be formed at room temperature. When syntheses are performed in reverse micelles, nanosized particles of $Cd_yZn_{1-y}S$ [22] and of Fe–Cu alloys [23]) are obtained.

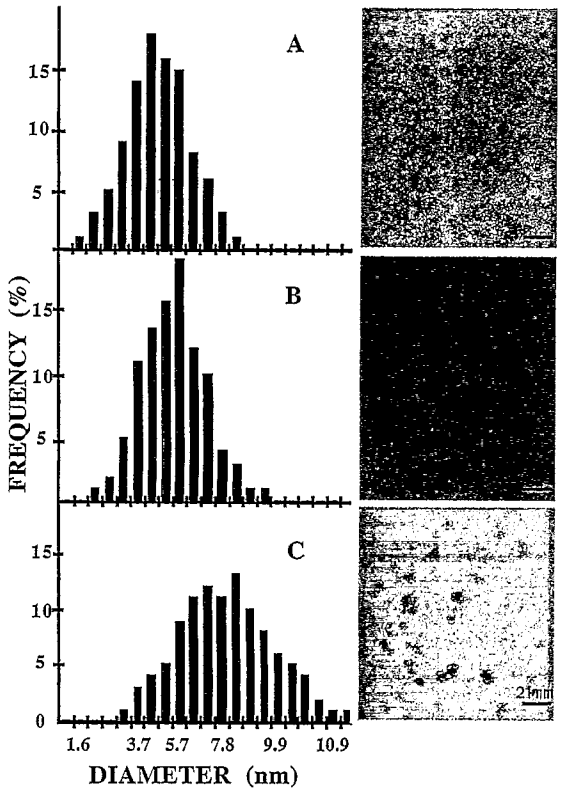

Fig. 1. Histogram of size and electron microscopy photograph of cobalt boride particles synthesized at: A, $w = 5$; B, $w = 7.5$; C, $w = 10$.

From the TEM patterns in Fig. 1, differences in the electronic contrast can be observed for particles made at water contents $w = 10$. A grey light coat surrounding higher-contrast material is observed. This change could be attributed to the formation of an oxide layer surrounding the Co_2B particles, which seems to appear during the transfer of the sample from the glovebox to the TEM apparatus.

High-resolution electron microscopy shows a well developed crystalline phase for these particles. Fig. 3 reveals the lattices fringes of the cobalt boride nanoparticles (tetragonal phase). No oxide shell can be observed, probably due to the lower crystallinity of the shell.

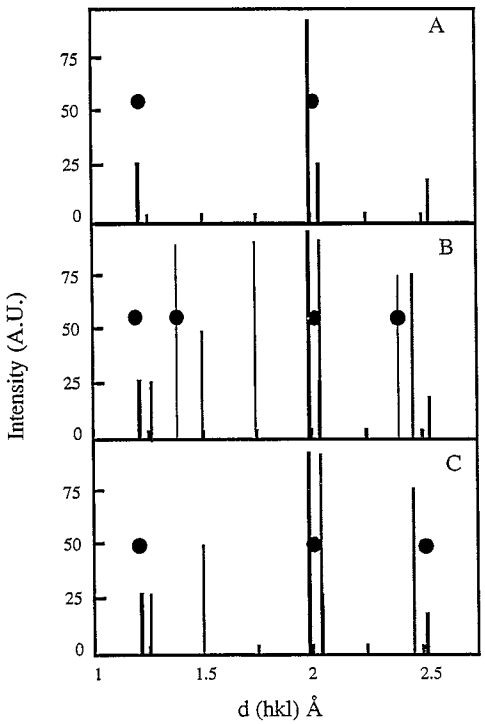

Fig. 2. Electron diffraction patterns of nanoparticles obtained at: A, $w = 5$ or 7.5; B, $w = 10$ before extraction; C, $w = 10$ after extraction. The lines refers to the ASTM files for Co_2B (large lines), CoO (narrow lines) and Co_2O_3 (grey lines).

The formation of cobalt boride can be explained by the following chemical scheme proposed for the aqueous solution [17]:

$$2BH_4^- + 2Co^{2+} + 2H_2O \rightarrow Co_2B + HBO_2 + 2H^+ + 4.5H_2$$

Fig. 4 shows the absorption spectra of cobalt boride obtained in a micellar solution and characterized by TEM (Fig. 1). The absorption spectra corresponding to various particle sizes are monotonous with a continuous increase in the optical density from 650 to 250 nm. The simulated absorption spectrum of metallic cobalt particles does not change with the particle size and is monotonous (inset, Fig. 4). Thus, the cobalt boride absorption spectrum shows behavior similar to that predicted for pure metallic cobalt particles [18], and does not change dramatically with the size of the particles.

When the solution is left in air, the overall absorption spectrum decreases, with the appearance of a peak at 350 nm and no residual absorption at 550 nm (Fig. 4). The shoulder at 350 nm can be attributed to cobalt oxide particles.

The kinetics of cobalt boride oxidation was followed at 550 nm. The increase in the first-order kinetic rate constant with the water content (Table 1) can be attributed to changes in the water structure: at low w values, water molecules are strongly bound at the interface and do not act as an oxidation agent. Similar results have been observed with metallic copper particles [11].

To compare the stability with the salt used to induce the chemical reaction, cobalt (2-ethyl hexyl) sulfosuccinate, $Co(AOT)_2$, was replaced by cobalt chloride, $CoCl_2$. At a given water content, it is observed a faster oxidation of cobalt boride with cobalt chloride than with AOT derivative. The increase in the particle stability when the salt is replaced by functionalized surfactant can be attributed to the fact that the cobalt ion is associates strongly

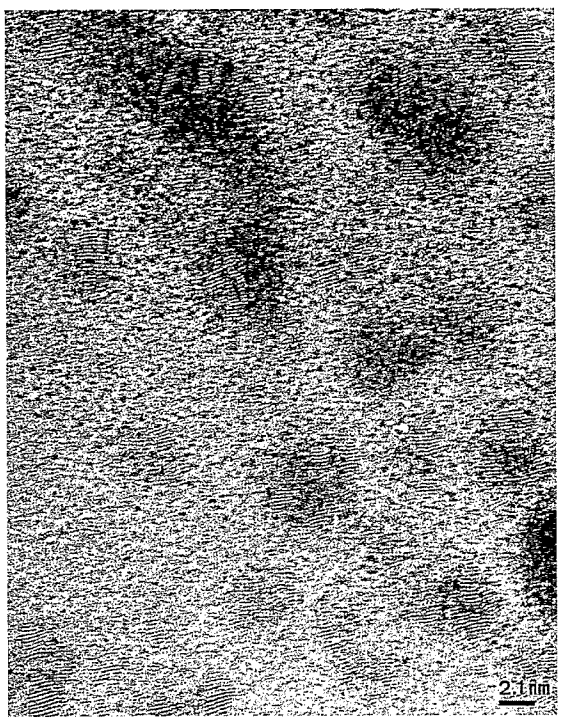

Fig. 3. High-resolution electron diffraction pattern of Co_2B nanosized particles ($w = 10$).

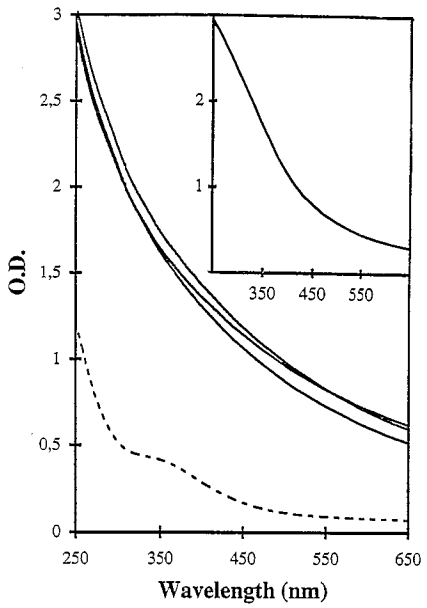

Fig. 4. UV–vis absorption spectra of cobalt particles $[NaBH_4]=0.02$ M; $[Co(AOT)_2]$ 0.005 M; [AOT] = 0.25 M. Experimental data at various water contents ($w = 5$–10). The dashed line is the absorption of $w = 7.5$ after complete reoxygenation. Inset: theoretical spectrum for pure metallic cobalt particles as calculated from Ref. [18].

with the interface, which plays an important role in the growth process. Similar behavior has been observed with silver [4] and copper [11] particles.

4.1.2. $w = \leq 2.5$

At water contents below $w = 2.5$, the addition of sodium borohydride does not change the absorption spectrum obtained with the $Co(AOT)_2/Na(AOT)/H_2O$ micellar solution. This indicates that no reduction of cobalt ions occurs at such low water contents. This could be attributed to the water structure, which is strongly bound at the interface and prevents the hydration of cobalt ions [24].

Table 1
Oxidation rate constants of cobalt boride particles depending on the mode of synthesis. [AOT] = 0.25 M, $[Co^{2+}]=5\times10^{-3}$ M, $[NaBH_4]=2\times10^{-2}$

Salt	Water content, w	k_{ox} ($\times10^4$ s^{-1})
$Co(AOT)_2$	5	7
$Co(AOT)_2$	7.5	11
$Co(AOT)_2$	10	10
$CoCl_2$	10	24

4.1.3. $w \geq 15$

At water contents up to 15, the particles formed are not stable in solution, and flocculate. This kinetic process increases with the water content.

4.2. Synthesis and characterization of Co_2B particles in a diphasic system

When a 0.1 M of $Co(AOT)_2$–isooctane micellar solution was added to an equal volume of 0.4 M $NaBH_4$ aqueous solution with vigorous stirring, a black precipitate appeared. This was washed with isooctane and then with acetone, and then dried under an argon atmosphere. Fig. 5 shows that the average particle diameter is 10 nm, with a large size distribution (40%).

Electron diffraction in various parts of the carbon grid did not give the same results. In some parts we observed the electron diffraction pattern of Co_2B, as shown in Fig. 2C. In other parts of the grid, spacings at 2.43, 2 and 1.5 were observed. These are close to the main spacing of CoO, indicating the formation of inhomogeneous materials made of Co_2B and Co–O.

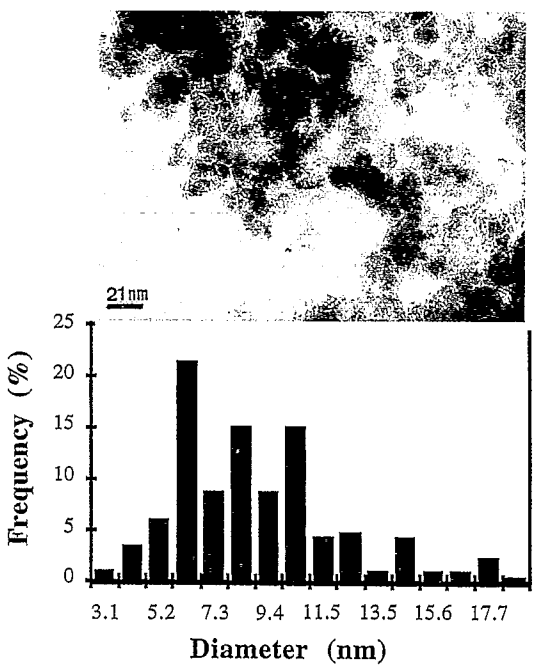

Fig. 5. TEM image and size histogram of Co_2B obtained by mixing the same volumes of an aqueous solution containing $NaBH_4$ (0.4 M), and a 0.1 M $Co(AOT)_2$/isooctane micellar solution.

In contrast with the reverse micellar solution, this method gives a large amount of material.

5. Magnetic properties

The commercial alternating gradient magnetometer used to study the magnetic properties does not allow the study of liquids. The experiments were therefore performed at room temperature using dry particles extracted and protected by a matrix of surfactant.

Cobalt boride particles were extracted from the micellar solution by mixing volume to volume the micellar solution and acetone [13]. The addition of a small amount of water molecules induced the immediate flocculation of the particles, which were then filtered, washed with acetone and dried under an argon atmosphere. With this method, all the cobalt boride particles (13.5 mg for 50 cm^3 of micellar solution) are recovered. The total weight of the black powder (around 100 mg) greatly exceeds the maximum weight of cobalt boride particles estimated from the initial concentration of cobalt ions (5×10^{-3} M). This indicates that a large amount of AOT remained in the sample (about 85%). The same results were obtained for all samples synthesized in AOT reverse micelles.

The particle size determined from TEM before and after extraction from the micellar solution did not change drastically in the size and polydispersity (Table 2), although some differences were observed. At water contents $w = 7.5$ and 10, the particle size was smaller than that observed before extraction (Table 2), whereas no changes were observed at $w = 5$. A comparison of the TEM patterns observed

Table 2
Size distribution of Co_2B, as observed by TEM in reverse micelles; and by TEM after extraction. For synthesis in micelles, [AOT] = 0.25 M, $[Co^{2+}] = 5 \times 10^{-3}$ M, $[NaBH_4] = 2 \times 10^{-2}$ M. For synthesis in diphasic systems, $[Co^{2+}] = 0.1$ M, $[NaBH_4] = 0.4$ M

Sample	In reverse micelles			After extraction	
	w	D (nm)	σ (%)	D (nm)	σ (%)
A	5	4.4	26	4	29
B	7.5	5.5	25	4	21
C	10	7.5	25	5	22
D	–	–	–	10	40

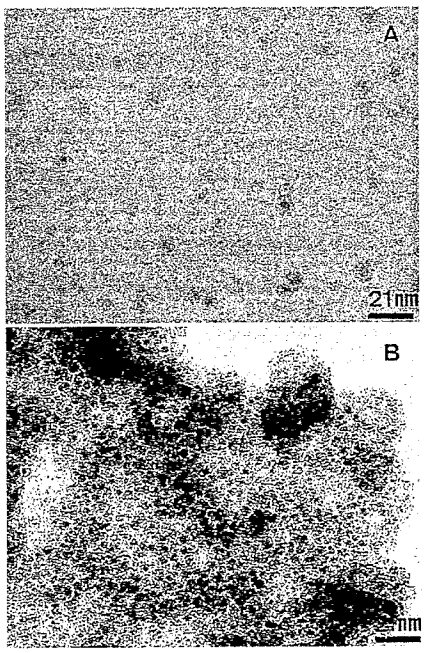

Fig. 6. TEM images of Co_2B particles before (A) and after (B) extraction of the microemulsion ($w = 10$).

before and after extraction (Fig. 6) shows that the layer surrounding the particle and attributed above to Co_2O_3, has disappeared. This was confirmed by the change in the diffraction patterns observed before (Fig. 2B) and after extraction (Fig. 2C). The appearance of such layer is due to oxidation, which occurs during the transfer of the sample in the reverse micelles from the glovebox to the TEM apparatus. It should be noted that, after extraction, the cobalt boride nanoparticles are uniformly dispersed in the AOT matrix (Fig. 6), which protects the sample from further oxidation. This is confirmed by the fact that no changes were observed in the magnetization curves after the particles were stored in air for one month.

Because of these differences in size, the particles made in the reverse micelles at $w = 5$, 7.5 and 10 are referred to as particles A, B and C, respectively (Fig. 1), and particles D were made in the diphasic system (Fig. 5). For particles A, B and C, the amounts of material obtained were very low. This induces a large error in the weight of the powder used. In contrast, the precision in the weight of particles D was good.

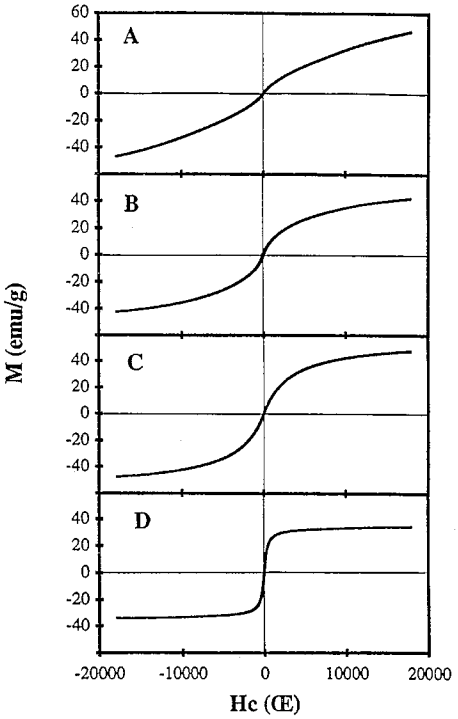

Fig. 7. Magnetization as function of the applied field at room temperature of the powder obtained after synthesis at various water contents and after extraction. A, $w = 5$; B, $w = 7.5$; C, $w = 10$; D, magnetization curve obtained with large Co_2B particles (10 nm).

Fig. 7 shows the magnetization curves, M (emu/g) versus H (Oe), obtained at room temperature for particles A, B, C and D. As expected, the magnetic field needed to reach saturation magnetization depends on the size of the particles: the smallest particles require the highest fields to reach saturation.

For particles A, saturation is not reached even for a magnetic field of 20 kOe, whereas it is reached for particles B. The saturation magnetizations of particles A, B and C, deduced from zero extrapolation of M versus $1/H$ [13], are of the same order of magnitude and equal to 60 ± 10 emu/g (Table 3). This is consistent with the bulk value for Co_2B given in Ref. [20]. The uncertainty in the saturation magnetization can be attributed to the accuracy of the measurement of the weight of the powder. Because of the experimental mode, the amount of cobalt boride obtained is very low. For particles D, a lower saturation magnetization compared to smaller size particles is obtained (Fig. 7D). This can be attributed to the presence of cobalt oxide, CoO, which is antiferromagnetic and induces a decrease in the magnetization.

Particles A, B and C show low coercivity values (35–70 Oe), which do not change dramatically with the particle size (Table 3). Because the particle size and the coercivity are very low compared with bulk Co_2B ($H_c \approx 2000$ Oe [20]), and the initial slope of the magnetization (i.e. the initial magnetic susceptibility, χ_0) depends strongly on the average particle size (Fig. 7), then to a first approximation, we assume superparamagnetic behavior. The coercivity can be attributed to the close proximity of the nanosized particles in the matrix (see Fig. 6B). This induces strong magnetic dipolar interactions between particles, which behave as having a larger size with a small coercivity. As expected, the coercivity increases with the size of the particles.

Strong evidence for superparamagnetic behavior is the change in the initial magnetic susceptibility, χ_0, with the size of the sample (Table 3). If the particles are superparamagnetic, the initial susceptibility must depend on the volume of the particles [21]:

$$\chi_0 \approx \left(M_s^2 V\right)/(3kT)$$

Fig. 8 shows a linear increase in χ_0 with the average volume of the particles for samples A, B and C. Thus these samples show superparamagnetic behavior at room temperature.

The susceptibility of sample D does not follow this linear dependence. This can be attributed to its large size and dispersion. Hence particles D are

Table 3
Magnetic properties of Co_2B nanoparticles obtained from AOT reverse micelles. [a] indicates that the magnetic diameter and dispersion were deduced from simulations of the first magnetization curves for samples A, B and C (see text)

Sample	M_s (emu/g)	H_c (Oe)	D [a] (nm)	σ (%)	χ (emu·g^{-1} Oe^{-1})
A	70 ± 10	35	2.6	35	$(4.5 \pm 1) \times 10^{-3}$
B	50 ± 5	75	4.4	28	$(10 \pm 3) \times 10^{-3}$
C	55 ± 5	35	5.4	29	$(18 \pm 5) \times 10^{-3}$
D	35 ± 5	55	–		$(60 \pm 5) \times 10^{-3}$

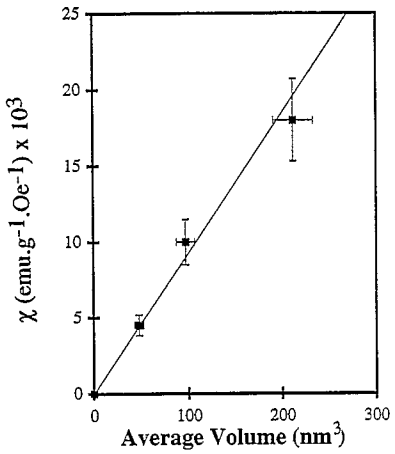

Fig. 8. Variation of the magnetic susceptibility, χ, with the volume of Co_2B particles.

ferromagnets at room temperature. This is consistent with the results of Chen et al. [13], which showed that cobalt particles of 10 nm are ferromagnetic at room temperature, whereas 4 nm particles are superparamagnetic

Because of the superparamagnetic behavior of samples A, B and C, the average magnetic size of the particle can be deduced from a simulation of Langevin relationship, assuming a log-normal size distribution from the first magnetization curve (Fig. 9) [16]. Good agreement between the size determined by TEM and from the magnetization curve is observed (Table 2). The magnetic diameter is lower than the physical diameter as determined in reverse micelles; this can be attributed to a 'dead layer' at the interface of the particles [22].

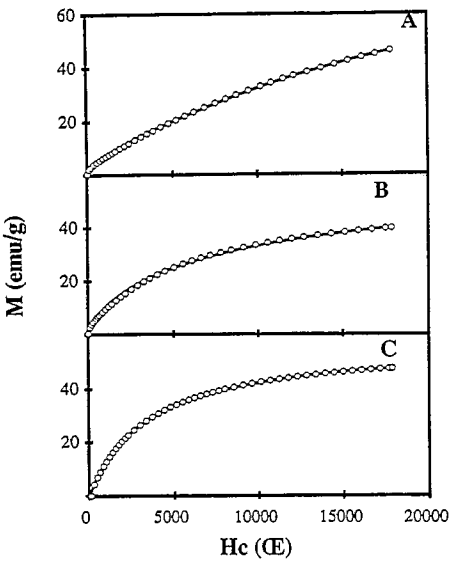

Fig. 9. First magnetization curve, at room temperature, of the powder obtained after synthesis at various water contents and after extraction: A, $w = 5$; B, $w = 7.5$; C, $w = 10$. The solid line is the best fit calculated from the Langevin equation assuming superparamagnetic particles.

6. Conclusions

Nanosized particles of cobalt boride, Co_2B, have been synthesized in situ in AOT reverse micelles, by the chemical reduction of cobalt ions by sodium borohydride. The use of a functionalized surfactant allows us to synthesize monodispersed particles of calibrated size depending on the micellar size. They are more stable than similar particles obtained with conventional salt. The particles can be extracted from the reverse micelles, maintaining their individual sizes. Superparamagnetic behavior is deduced from the analysis of the initial susceptibility of the smallest particles, whereas the largest particles show ferromagnetic behavior. The magnetization at saturation is close to that of bulk Co_2B. Simulation of the first magnetization curve, confirms the observed size distribution and the micellar size effect on the synthesis of Co_2B nanoparticles.

Acknowledgements

We wish to thank Dr B. Barbara for fruitful discussions, and for a critical reading of this manuscript.

References

[1] For a review, see G.A. Ozin, Adv. Mater. 4 (1992) 612.
[2] M.P. Pileni, L. Motte and C. Petit, Chemistry of Materials 4 (1992) 338.
[3] See M.G. Bawendi, M.L. Steigerwald and L.E. Brus, Ann. Rev. Phys. Chem. 41 (1990) 477, and references therein.
[4] C. Petit, M.P. Lixon and M.P. Pileni, J. Phys. Chem. 97 (1993) 12974.
[5] See A. Henglein, Chem. Rev. 89 (1989) (1861).

[6] M.L. Billas, I.A. Châtelain and W.A. de Heer, Science 265 (1994) 1682.
[7] For a review see: M.P. Pileni, J. Phys. Chem. (1993); V. Pillai, P. Kumar, M.J. Hou, P. Ayyub and D.O. Shah, Adv. Colloid. Interface. Sci. 55 (1995) 241, and references therein.
[8] M.P. Pileni (Ed.), Structure and Reactivity in Reverse Micelles (Elsevier, Amsterdam, 1989).
[9] M.P. Pileni, T. Zemb and C. Petit, Chem. Phys. Lett. 118 (1985) 414.
[10] C. Petit and M.P. Pileni, J. Phys. Chem. 92 (1988) 4734.
[11] I. Lisiecki and M.P. Pileni, J. Am. Chem. Soc. 115 (1993) 3887.
[12] J.P. Chen, K.M. Lee, C.M. Sorensen, K.J. Klabunde, and G.C. Hadjipanayis, J. Appl. Phys. 75 (1994) 5876.
[13] J.P. Chen, C.M. Sorensen, K.J. Klabunde and G.C. Hadjipanayis, J. Appl. Phys. 76 (1994) 6316.
[14] C. Petit, P. Lixon and M.P. Pileni, Langmuir 7 (1991) 2620.
[15] P. Bacri, R. Perzinsky, V. Cabuil and R. Massart, J. Magn. Magn. Mater. 62 (1986) 36.
[16] G. Cassin, J.P. Badiali and M.P. Pileni, J. Phys. Chem. 99 (1995) 12941.
[17] J. Shen, Z. Li, Q. Yan and Y. Chen, J. Phys. Chem. 97 (1993) 8504.
[18] J.A. Creighton and D.G. Eaton, J. Chem. Soc, Faraday Trans. II 87 (1991) 3881.
[19] JCPDS, Int. Centre for Diffraction Data, No. 25-0241.
[20] Y. Yiping, G.C. Hadjipanayis, C.M. Sorensen and K.J. Klabunde, J. Magn. Magn. Mater. 79 (1989) 321.
[21] J.L. Dorman, Rev. Phys. Appl. 16 (1981) 275.
[22] J. Cizeron and M.P. Pileni, J. Phys. Chem. 99 (1995) 17410.
[23] N. Duxin and M.P. Pileni, to be published.
[24] L. Motte, I. Lisiecki and M.P. Pileni, in: Hydrogen Bond Network, eds. M.C. Bellissent-Funel and J.C. Dore, NATO ASI Ser. C, vol. 435 (Kluwer, Dordrecht, 1994) p. 447.